Published in final edited form as:

Curr Biol. 2021 May 24; 31(10): 2099–2110.e5. doi:10.1016/j.cub.2021.02.055.

Retrorubral field is a hub for diverse threat and aversive outcome signals

Mahsa Moaddab[*], **Michael A. McDannald**[*,#]

Boston College, Department of Psychology & Neuroscience, 140 Commonwealth Avenue, 514 McGuinn Hall, Chestnut Hill, MA 02467, USA

SUMMARY

Adaptive fear scales to degree of threat and requires diverse neural signals for threat and aversive outcome. We propose the retrorubral field (RRF), a midbrain region containing A8 dopamine, is a neural origin of such signals. To reveal these signals, we recorded RRF single-unit activity while male rats discriminated danger, uncertainty, and safety. Many RRF neurons showed firing extremes to danger and safety that framed intermediate firing to uncertainty. The remaining neurons showed unique, threat-selective cue firing patterns. Diversity in firing direction, magnitude and temporal characteristics led to the detection of at least eight, functional neuron types. Neuron types defined with respect to threat showed unique firing patterns following aversive outcome. The result was RRF signals for foot shock receipt, positive prediction error, anti-positive prediction error, persistent safety, and persistent threat. The diversity of threat and aversive outcome signals points to a key role for the RRF in adaptive fear.

eTOC Blurb

Moaddab and McDannald show that retrorubral field neurons signal diverse aspects of threat cues and aversive outcome through variations in firing pattern, timing, direction and magnitude. The results reveal the retrorubral field is a hub for signals to shape fear behavior.

Keywords

A8; Dopamine; Fear; Safety; Single unit; Associative learning; Conditioned suppression

[*]Corresponding Authors: Please address correspondence to M.M. (moaddab@bc.edu) or M.A.M. (michael.mcdannald@bc.edu).
[#]Lead contact

AUTHOR CONTRIBUTIONS

Conceptualization, M.A.M.; Methodology, M.M. and M.A.M.; Investigation, M.M.; Writing – Original Draft, M.M. and M.A.M.; Writing – Review & Editing, M.M. and M.A.M.; Funding Acquisition, M.A.M.; Resources, M.A.M.; Visualization, M.M. and M.A.M.; Supervision, M.A.M.

Michael A. McDannald twitter handle: @mikemcdannald
Mahsa Moaddab twitter handle: @MahsaMoaddab
McDannald lab twitter handle: @mcdannaldlab

DECLARATIONS OF INTERESTS

The authors declare no competing interests.

INTRODUCTION

Fear in the face of certain danger is adaptive. Early studies identified an essential role for the amygdala in danger-elicited fear[1–4]. This success has spawned systematic study of amygdalar contributions to fear that continues today[5–7]. Yet, real world threats typically involve uncertainty [8,9], and adaptive behavior requires the level of fear to scale to degree of threat. Adaptive fear almost certainly requires a larger threat network[10,11], with critical network nodes signaling diverse aspects of threat[12–14] and aversive outcome[14–18]. Identifying these nodes is essential to mapping a complete threat network for adaptive fear.

Anatomical position, neuron-type composition and projection profile make the retrorubral field (RRF) a compelling candidate for a critical threat network node. The RRF is a midbrain region situated dorsal and posterior to the substantia nigra (SN). The RRF is perhaps best known as the source of A8 dopamine[19–22], the third largest dopamine group behind the A10 ventral tegmental area (VTA) and A9 SN groups[23,24]. The RRF also contains γ-aminobutyric acid (GABA)[24] and glutamate neurons[25,26] that likely contribute to distinct, yet complementary behavioral processes[27,28]. The RRF is anatomically poised to interact with a larger threat network. RRF neurons, including A8 dopamine, directly project to regions essential to fear, including medullary/pontine regions[29], the central amygdala[1,3], nucleus accumbens core[30,31], ventral pallidum[32,33], bed nucleus of the stria terminalis[34,35], and hippocampus[36,37]. Indeed, RRF neuron-type composition and connectivity have led to previous proposals for a role in fear[38,39].

Despite its candidacy as a critical threat network node, little is known of RRF threat function. The goal of the current study was to comprehensively reveal RRF threat and aversive outcome signaling. RRF single-unit activity was recorded while male rats underwent fear discrimination consisting of cues predicting unique foot shock probabilities: danger ($p = 1.00$), uncertainty ($p = 0.25$), and safety ($p = 0.00$). Using this procedure, we find that rats utilize threat probability to guide fear behavior, fully discriminating the three cues[15,15,40–43]. The behavior/recording approach allowed us to specify RRF threat signaling by analyzing single-unit activity during cue presentation; and to specify aversive outcome signaling by analyzing single-unit activity following foot shock delivery or omission.

RESULTS

Eleven male Long Evans rats were mildly food deprived and shaped to nose poke for a pellet reward. Nose poking was reinforced throughout testing, but poke-reward and cue-shock contingencies were separate. Rats received eight initial fear discrimination sessions (Figure 1A) in which three, 10-s auditory stimuli predicted unique foot shock probabilities: danger ($p = 1.00$), uncertainty ($p = 0.25$), and safety ($p = 0.00$). Each session consisted of four danger trials, eight uncertainty trials (two with foot shock) and four safety trials, with trial order randomized. Fear was measured by the suppression of rewarded nose poking, comparing nose poke rates during baseline and cue periods[44,45] (see STAR Methods). Suppression of rewarded nose poking was used because it is an objective, continuous measure of fear output[46,47] that correlates with the more common measure of freezing[48].

Nose poke suppression provided a precise trial-by-trial measure of fear output, which was required for regression analyses.

Following the eighth discrimination session, rats were returned to *ad libitum* food access and underwent stereotaxic surgery. Drivable microelectrode bundles were implanted just dorsal to the RRF region containing A8 dopamine neurons. Following recovery, rats were again food deprived and returned to fear discrimination, now while recording RRF single-unit activity. Single units were isolated prior to each recording session and held for the session duration. The microelectrode bundle was advanced ~80 μm between sessions in order to record from the full RRF dorsal-ventral extent. Rats showed complete behavioral discrimination during the sessions from which the single units of interest were obtained (Figure 1B). ANOVA for suppression ratio revealed a main effect of cue ($F_{2,20} = 103.57$, $p = 2.80 \times 10^{-11}$, $\eta p^2 = 0.91$, op = 1.00). We used 95% bootstrap confidence intervals to examine differential suppression ratios for each cue pair, and for differential firing/signaling throughout the manuscript. The null hypothesis states that differential suppression ratios (or differential firing/signaling) were not observed. The null hypothesis is rejected if the 95% bootstrap confidence interval – defined by its lower and upper bounds – does not contain zero. 95% bootstrap confidence intervals for differential suppression ratios did not contain zero for any cue comparison: danger vs. uncertainty (mean = 0.42, 95% CI [(lower bound) 0.34, (upper bound) 0.56]); uncertainty vs. safety (M = 0.40, 95% CI [0.06, 0.53]); and danger vs. safety (M = 0.82, 95% CI [0.75, 0.94]). Observing complete behavioral discrimination permits a rigorous examination of RRF threat and aversive outcome responding.

At the conclusion of testing, rats were perfused, brains frozen, sliced and sections processed with immunohistochemistry for tyrosine hydroxylase, a dopamine marker (Figure 1C). Only single units originating from anterior-posterior and dorsal-ventral locations containing tyrosine hydroxylase staining of A8 dopamine neurons were considered for analysis. Single units were collected across the entire RRF anterior-posterior span (−6.36 to −7.08; Figure 1D), though most single units were collected from bregma levels −6.72 and −6.84. Single units were not collected from adjacent brain regions including: the SN, pedunculopontine tegmental nucleus and pararubral nucleus.

Diverse cue firing patterns

We recorded 743 single units from 11 rats over 228 fear discrimination sessions. We screened each single unit for cue responsiveness by comparing baseline firing rate (mean of 10 s prior to cue onset) to firing rates during cue onset (first 1 s) and late cue (last 5 s) for danger, uncertainty, and safety (paired t-test, $p < 0.05$). Single units showing significant firing increases or decreases to any cue, relative to baseline, were considered cue responsive. Four hundred and twenty-three cue-responsive single units were obtained from 190 sessions, and no fewer than 11 single units were identified per rat (Figure S1).

There was considerable diversity in the pattern of cue and aversive outcome responding, suggesting that single units could be divided into distinct, functional populations. To reveal these populations, we summarized normalized firing rate in a 423 single unit x 54 epoch matrix. The 54 epochs were taken from the 10, 1-s cue intervals (danger, epochs 1-10;

uncertainty, epochs 11-20; and safety, epochs 21-30) and from 6, 1-s intervals following foot shock delivery and omission (danger, epochs 31-36; uncertainty shock, epochs 37-42; uncertainty omission, epochs 43-48; and safety, epochs 49-54). We applied k-means clustering to the matrix, incrementing the number of clusters from 1 to 15, and determining the mean of the squared Euclidean distance for each cluster member from its centroid (Figure 1E). As expected, Euclidean distance from centroid decreased as cluster number increased, with the amount of decrease diminishing after a cluster number of eight. Eight clusters grouped similar functional types, while six and seven clusters grouped dissimilar types, and nine and ten clusters divided the main functional types into smaller subtypes (Figure S2). All subsequent analyses consider eight clusters: k1, n = 33; k2, n = 59; k3, n = 18; k4, n = 63; k5, n = 58; k6, n = 61; k7, n = 64; and k8, n = 67.

Single-unit function was minimally related to anterior-posterior recording location and firing characteristics (Figure 1F). Multiple analysis of variance (between subjects factor: cluster) for dependent measures of anterior-posterior recording location (Figure 1F, top), baseline firing rate (Hz; Figure 1F, bottom), waveform half duration, waveform amplitude ratio, coefficient of variance and coefficient of skewness (Figure S3) found a main effect of cluster for baseline firing rate ($F_{7,415} = 2.48$, $p = 0.017$, $\eta p^2 = 0.04$, op = 0.88), coefficient of variance ($F_{7,415} = 2.28$, $p = 0.027$, $\eta p^2 = 0.04$, op = 0.84), and coefficient of skewness ($F_{7,415} = 2.65$, $p = 0.011$, $\eta p^2 = 0.04$, op = 0.90). The single units comprising clusters k1 and k3 had lower baseline firing rates compared to all other clusters ($t_{421} = 3.28$, $p = 0.001$).

In order to visualize firing patterns (Figure 2), we organized units by cluster and plotted mean cue and aversive outcome firing. Single units from each cluster showed a unique differential cue firing pattern. In support, ANOVA for normalized firing rate [factors: cue (danger, uncertainty, and safety) and interval (56, 250 ms bins: 2-s baseline → 10-s cue → 2-s delay)] found a significant trial type x interval interaction for each cluster (Table 1). Neuronal clusters were primarily defined by their responses to danger and uncertainty. Roughly half of RRF single units (clusters k1, k3, k5, and k7; Figure 3A, B) showed excitatory firing to danger and uncertainty, though with varying magnitudes and distinct temporal characteristics. K1 neurons were strongly cue onset responsive, firing maximally to danger but firing at lower and similar levels to uncertainty and safety. K3 neurons sustained differential firing throughout cue presentation and the 2-s delay period (between cue offset and shock onset): danger > uncertainty > safety. K5 neurons ramped danger and uncertainty firing, fully differentiating the three cues by the last half of cue presentation: danger > uncertainty > safety. K7 neurons were minimally cue responsive, but showed complete differential cue firing during the 2-s delay period: danger > uncertainty > safety. The remaining RRF single units (clusters k2, k4, k6, and k8; Figure 3C, D) showed unique inhibitory firing patterns that were sustained throughout cue presentation and the 2-s delay period. K2 neurons specifically inhibited firing to uncertainty. K4 neurons specifically and equivalently inhibited firing to danger and uncertainty. K6 neurons were maximally inhibited to danger, less strongly inhibited to uncertainty but showed excitatory firing to safety. K8 neurons specifically inhibited firing to danger. 95% bootstrap confidence intervals confirmed the description of each cluster's differential firing (Table S1). Data visualization and 95% confidence intervals (Figure S4) for change in firing [delay – onset] confirm phasic, onset

firing increases for all cues by k1 neurons, and ramping firing increases for danger and uncertainty by k5 neurons.

Uniform firing bias towards threat cues

The diversity of RRF cue responding was most apparent when mean danger firing was plotted for each cluster (Figure 4A; clusters plotted separately in Figure S5). The eight clusters showed considerable variation in the direction, magnitude and temporal characteristics of danger firing. Considering danger firing alone severely diminishes ones hope of identifying a uniform response pattern in RRF neurons. Yet, when mean uncertainty firing (Figure 4B) and safety firing (Figure 4C) were examined, a uniform threat bias was apparent. With the exception of cluster k2, the direction and temporal characteristics of each cluster's uncertainty firing was similar to that for danger, only diminished in magnitude. Critically, across all eight clusters, safety firing direction tended to *oppose* danger firing direction. Clusters k4 and k6 showed considerable firing inhibition to danger, but firing increases to safety. Just the opposite was observed for clusters k3 and k5, which showed firing increases to danger, but firing inhibitions to safety.

In support, there was a positive relationship between danger and uncertainty firing across all clusters during each period (Figure 4D–F): onset ($R^2 = 0.48$, $p = 3.25 \times 10^{-62}$), late cue ($R^2 = 0.21$, $p = 8.23 \times 10^{-24}$), and delay ($R^2 = 0.21$, $p = 2.46 \times 10^{-23}$). Smaller and even opposing firing relationships were observed for danger and safety (Figure 4G–I). There was positive relationship between danger and safety firing at cue onset ($R^2 = 0.14$, $p = 7.98 \times 10^{-16}$), but negative relationships were observed during late cue ($R^2 = 0.03$, $p = 1.48 \times 10^{-4}$) and delay ($R^2 = 0.02$, $p = 0.008$). Importantly, Fisher r-to-z transformation revealed the danger-uncertainty and danger-safety relationships differed from one another during each period: onset ($Z = 7.69$), late cue ($Z = 8.94$) and delay ($Z = 8.20$) (test could not provide specific *p*-values, instead returned 0.00 for each; see STAR Methods).

The most common RRF firing pattern (|danger > uncertainty > safety|) roughly approximated the fear discrimination pattern (danger > uncertainty > safety), meaning RRF neurons may signal fear output. The relative firing pattern also roughly approximated each cue's foot shock probability, in which case RRF neurons may be precisely tuned to threat probability. However, the profound threat firing bias – with uncertainty firing levels approaching danger levels – may mean that RRF neurons are tuned to an exaggerated threat probability. Given the diversity of cue firing, signaling and tuning are likely to vary across clusters.

Exaggerated threat probability signaling

To distinguish these possibilities and reveal cluster-specific threat tuning, we performed linear regression for single units comprising each cluster. For each single unit, we calculated the normalized firing rate for each trial (16 total: 4 danger, 8 uncertainty, and 4 safety) in 1-s bins over the 10-s cue. The trial-specific suppression ratio was used as the fear output regressor. The threat probability regressor assigned numerical values to each cue. The values assigned to danger (1) and safety (0) were fixed, but the value assigned to uncertainty was incremented from 0 to 1 in 0.125 steps (0.000, 0.125, 0.250, 0.375, 0.500, 0.625, 0.750,

0.875, and 1.000). K2 neurons were omitted from regression analysis because their firing pattern violated the assumption that uncertainty firing fell between the bounds of danger and safety (Figure S5C and D). Regression output was a beta coefficient quantifying the strength (|>0| = stronger) and direction (>0 = positive) of the predictive relationship between each regressor and single-unit firing. A threat tuning curve (Figure 5A) was constructed for each cluster by averaging the threat probability beta coefficient for each uncertainty assignment. Averages were taken from the cluster-specific cue periods identified in Figure 3A and C. Beta coefficient values were inverted (value*-1) for cue-inhibited clusters k4, k6, and k8, so that signaling would be indicated by positive values for all clusters.

RRF neurons in clusters k1, k3, k5, and k7 showed exaggerated threat probability signaling (Figure 5A). That is, the firing level to uncertainty was disproportionate to the foot shock probability assigned to the uncertainty cue (0.250). In support, tuning curve peaks exceeded 0.250: k1, k3, k5 = 0.375 and k7 = 0.500. These peaks were closer to the mean fear level demonstrated to the uncertainty cue. RRF neurons in clusters k4, k6, and k8 showed greater variation in their tuning (Figure 5A). K4 and k6 neurons showed even greater exaggeration of threat probability signaling. Tuning curve peaks for each cluster were: k4 = 0.875, and k6 = 0.625, now exceeding even fear output. K8 neurons were more tuned to the actual shock probability, with a peak of 0.250 that flattened towards 0.000. Consistent with different firing magnitudes and non-identical tuning, ANOVA [factors: cluster (7) and assignment (9)] revealed a main effect of cluster ($F_{6,357} = 4.14$, $p = 0.0005$, $\eta p^2 = 0.07$, op = 0.98) and cluster x assignment interaction ($F_{48,2856} = 7.22$, $p = 1.16 \times 10^{-43}$, $\eta p^2 = 0.11$, op = 1.00). Demonstrative of uncertainty over-responding across clusters, ANOVA found a main effect of assignment ($F_{8,2856} = 24.84$, $p = 2.67 \times 10^{-37}$, $\eta p^2 = 0.07$, op = 1.00). Exaggerated threat probability signaling was visually apparent (Figure 5B) when values were expressed as the percent of the peak beta coefficient.

The tuning curves reveal that most RRF neurons do not precisely signal threat probability. However, the tuning curves cannot distinguish exaggerated threat probability signaling from fear output signaling, and cannot reveal the pattern of signaling over cue presentation. To determine each of these, we performed single-unit linear regression using peak threat probability and fear output as regressors. Regression was performed in 14, 1-s bins, starting 2 s prior to cue onset and continuing through the 2-s delay period. The mean beta coefficient for peak threat probability (Figure 5C) and fear output (Figure 5D) are plotted for each cluster. Neither peak threat probability nor fear output signaling was observed prior to cue onset. Across all seven clusters (Figure 5E), peak threat probability was continuously signaled from cue onset through delay. Fear output was signaled in all bins except for the first, however, peak threat probability signaling exceeded fear output signaling at each time point.

Revealing consistent peak threat probability signaling across clusters, ANOVA for beta coefficients [within factors: regressor (peak threat probability and fear output; between factors: cluster (7) and bin (14)] found a significant main effect of regressor ($F_{1,355} = 28.57$, $p = 1.62 \times 10^{-7}$, $\eta p^2 = 0.07$, op = 1.00) and a regressor x bin interaction ($F_{13,4615} = 4.13$, $p = 7.40 \times 10^{-7}$, $\eta p^2 = 0.01$, op = 1.00). 95% boot strap confidence intervals confirmed these descriptions (Table S2). Indicative of some variation between clusters (clusters plotted

separately in Figure S6; Table S3), ANOVA revealed a regressor x cluster interaction ($F_{6,355}$ = 2.15, p = 0.048, ηp^2 = 0.04, op = 0.76), but no regressor x cluster x bin interaction ($F_{78,4615}$ = 1.06, p = 0.33, ηp^2 = 0.02, op = 1.00). Peak threat probability and fear output were not discretely signaled by distinct RRF populations. A continuous, negative relationship (R^2 = 0.43, $p = 4.18 \times 10^{-46}$; Figure 5F) between fear output and peak threat probability signaling was observed across all neurons, with signaling biased towards peak threat probability.

Diverse aversive outcome firing patterns

Like for cue firing, there was considerable diversity in the pattern, direction, magnitude and temporal characteristics of firing for each cluster following the delivery and omission of aversive outcomes (Figure 6A–H). We plotted mean trial type activity to examine cluster firing patterns, now separating uncertainty shock and uncertainty omission trial types. Every cluster showed differential firing during the outcome period; ANOVA [factors: trial type (danger vs. uncertainty shock vs. uncertainty omission vs. safety) and interval (17.5-s post shock; 70, 250 ms bins)] found a main effect of trial type and/or a trial type x interval interaction for every cluster (Table 1). Differential firing was transient for some clusters, largely confined to the 4-6 s following shock delivery or omission. Differential firing was persistent for other clusters, with firing sustained for the entirety of the 17.5 s period. To visualize firing patterns (Figure 6, column i; Table 1 and Table S4), we plotted single-unit and mean trial type firing for each cluster from the relevant time period (grey outline in Figure 6A–H). To reveal differential firing patterns (Figure 6, column ii), we constructed and plotted 95% bootstrap confidence intervals for: [uncertainty shock – danger], [uncertainty omission – safety], and [danger – safety] for each cluster.

Trial type-specific firing patterns and confidence intervals for differential firing revealed unique aversive outcome responding by each cluster. K1 neurons (Figure 6A, i, ii) were generally shock responsive, showing equivalent and transient responding following danger and uncertainty shock. K2 neurons (Figure 6B, i, ii) fired maximally to the fully predicted shock on danger trials, but showed firing inhibition to the surprising shock on uncertainty trials; consistent with an anti-positive prediction error signal. K3 neurons (Figure 6C, i, ii) sharply reduced firing following shock, but sustained excitation of firing following omission on uncertainty trials, revealing a continued threat signal. K4 neurons (Figure 6D, i, ii) sustained firing inhibition on uncertainty omission trials, while k5 neurons (Figure 6E, i, ii) sustained firing increases; revealing similar sustained threat signaling through opposing firing directions. K6 neurons (Figure 6F, i, ii) showed early positive prediction error signaling through firing decreases: greater firing inhibition following shock delivery on uncertainty trials compared to danger trials. Early positive prediction error signaling gave way to a sustained valence signal with maximal firing to safety, little firing following shock omission, and sustained firing inhibition following danger and uncertainty shock. K7 neurons (Figure 6G, i, ii) showed initial valence signaling (danger shock = uncertainty shock > omission > safety) that gave way to positive prediction error (uncertainty shock > danger shock). Impressively, k7 neurons sustained firing inhibition to safety throughout the outcome period. Finally, k8 neurons (Figure 6H, i, ii) showed early positive prediction error signaling (uncertainty shock > danger shock) that gave way to an unsigned prediction error signal in

which equivalent firing increases on uncertainty shock and omission trials exceeded those for danger and safety.

DISCUSSION

We recorded RRF single-unit activity while rats underwent fear discrimination and observed diverse neural signals for threat and aversive outcome. Threat signals differentiated danger/uncertainty from safety, but showed considerable variation in their firing pattern, direction, magnitude and temporal characteristics. Aversive outcome signals were even more varied; ranging from shock delivery and prediction error-related responding to sustained threat and safety responding. Before discussing the results more broadly, several limitations should be noted.

The present results cannot tie neuron-type function to neurotransmitter identity. Historically, VTA/SN dopamine neurons have been identified by their firing characteristics: low baseline firing rates and wide waveforms with an initial hyperpolarization component[49]. K3 neurons, showing sustained danger and uncertainty firing increases, as well as sustained threat responding following shock omission, most closely matched this traditional baseline firing and waveform profile. Yet, K3 neurons did not have a strong initial hyperpolarization component, nor did any other functional type. A more recent approach combining transgenic mice and optogenetics finds that neurotransmitter identity (dopamine vs. GABA) can be inferred from reward function[50–52]. Now that we have shown specific signals for threat and aversive outcome, applying transgenic/optogenetic classification to the RRF may permit us to tie specific signaling to neurotransmitter identity.

Our recordings came exclusively from male rats. This was because our initial fear discrimination studies utilized males[42,43]. Studies providing critical insight to VTA dopamine contributions to reward and aversive learning have mainly used males[51,53–57], and no differences in VTA activity/function have been found in studies that used females and males[58–62]. These findings indicate that VTA dopamine neurons underlying core learning/decision signals may not meaningfully differ by sex. We anticipate the diverse signals we observe in male RRF neurons are present in females. One caveat is that threat tuning by RRF functional types may differ by sex. While we observe complete and comparable fear discrimination in both sexes, females tend to show higher fear to uncertainty[40].

The most robust finding was the diversity of RRF responses to threat cues and aversive outcomes. What can we make of such diversity? One possibility is that distinct functional types contribute to independent threat functions through unique projection profiles. Two broad functional types were observed during the cue period; neurons differentiating cues (clusters k3, k5, k6, and k7) and neurons categorizing cues (clusters k1, k2, k4, and k8). RRF neurons fully differentiating danger, uncertainty and safety may project to brain regions controlling fear output, such as the central amygdala[36] and medullary/pontine regions[29]. RRF neurons categorizing cues into danger, uncertainty and threat may project to brain regions that do not elicit fear *de novo* but shape adaptive fear responses, such as the nucleus accumbens[30] and ventral pallidum[32]. Yet, function-projection relationships will likely defy simplicity. Neurons fully differentiating cues showed divergent firing patterns following

aversive outcome; ranging from positive prediction error signaling to sustained threat and valence signaling. Neurons more simply categorizing cues showed complex and divergent firing patterns following aversive outcome; with signals for foot shock receipt, sustained threat, positive prediction error, anti-positive prediction error and unsigned prediction error apparent. While speculative, a function-projection framework is consistent with findings showing that specific VTA/SN dopamine and GABA projections underlie independent, threat and aversion functions[54,56,63–66]. Our observation of diverse signaling of threat and aversive outcome by RRF neurons is broadly consistent with diverse signaling of reward variables by VTA dopamine neurons[67].

A second possibility is that RRF neurons represent a ‘threat time’ population code. This idea borrows from the hippocampus, in which a robust time population code is constructed by having neurons tuned to different, specific temporal positions within a structured experience[68–70]. Hippocampal encoding of temporal structure is even observed across complex, sequential odor tasks[71]. By having RRF neurons with differing temporal firing patterns (onset, sustain, ramping), directionality (excitation vs. inhibition) and magnitude, a population code during cue presentation may inform the time to aversive outcome. Of interest, RRF neurons project directly to CA1[37], the hippocampal subfield in which time cells were first reported[68]. The threat time scheme may extend to the outcome period. Only now, a RRF population code may signal the passage of time since aversive outcome delivery or omission. Persistent safety signals may permit non-threat behaviors like foraging and grooming to continue, while persistent threat signals may prolong defensive behavior to prevent detection and reduce the likelihood of further harm. RRF neurons enjoy modest projections to the dorsomedial hypothalamus[36], which along with the ventromedial hypothalamus is necessary to sustain defensive behavioral states[72]. We also observed positive prediction error signals during the aversive outcome period, as well as the inverse of positive prediction error – selective firing to the predicted foot shock. Reward prediction error is ubiquitous in the VTA/SN[50,61,73–76], and our results suggest that prediction error-related firing may be a defining feature of dopamine-containing brain regions.

A consistent finding across many RRF neuron types was the level of uncertainty firing exceeded the uncertainty foot shock probability (i.e. uncertainty firing level was not 25% of the distance between danger and safety firing levels). RRF cue firing patterns were only minimally related to the behavioral pattern of fear discrimination – although RRF neurons could signal a fear output we did not measure[2,77,78]. Indeed, if RRF neurons alone were driving behavior, danger and uncertainty would elicit nearly identical fear levels. So what utility might an RRF-derived exaggerated threat probability signal serve? We think the ultimate answer is that an individual’s pattern of fear expression is the sum of many predictions, each reflecting a unique dimension of threat. Among several ventrolateral periaqueductal gray (vlPAG) functional types, we have observed one neuronal population that more precisely signals threat probability[12]. These vlPAG neurons linearly increased cue firing according to the actual foot shock probability. In our discrimination procedure, rats typically show a pattern of fear that is intermediate to the extremes that would be produced by only RRF or only vlPAG neurons. Threat predictions arising in the amygdala[79], prefrontal cortices [41,80,81], ventral pallidum[32], nucleus accumbens[30] and additional brain regions[10] likely interact with one another. Ultimately, these threat predictions may be fed to

the RRF and vlPAG, whose medullary and pontine projections summate to shape the complete fear discrimination pattern we observe[29,82].

Dopamine plays a central role in threat and aversion[56,83–90]. VTA/SN neurons have been viewed as the origin of dopamine signals governing fear. Undoubtedly, the VTA and SN are responsive to threat cues, and are critical for threat processes underlying fear behavior[59,91,92]. Yet, our results reveal that neurons originating in the RRF signal multiple, unique aspects of threat and aversive outcome. Determining the neurotransmitter identity, transcriptome[93] and projection profiles of these distinct RRF functional types – and their interactions with a larger neural network – will hasten a more complete understanding of the neural basis of adaptive fear.

STAR METHODS

RESOURCE AVAILABILITY

Lead contact—Further information and requests for resources and reagents should be directed to and will be fulfilled by the Lead Contact, Michael A. McDannald (michael.mcdannald@bc.edu).

Materials availability—This study did not generate new unique reagents.

Data and code availability—Full electrophysiology data set and MATLAB code will be uploaded to http://crcns.org/ upon acceptance for publication.

EXPERIMENTAL MODEL AND SUBJECT DETAILS

Adult male Long Evans rats, weighting 250–275 g, were obtained from Charles River Laboratories (n = 14, Raleigh, NC). Rats were individually housed and maintained on a 12 h light cycle (lights off at 6:00 p.m.) with free access to water. Rats were maintained at 85% of their free-feeding body weight with except during surgery and post-surgery recovery periods where animals had *ad libitum* access to food (standard laboratory chow, 18% Protein Rodent Diet #2018, Harlan Teklad Global Diets, Madison, WI). All protocols were approved by the Boston College Animal Care and Use Committee, and all experiments were carried out in accordance with the NIH guidelines regarding the care and use of rats for experimental procedures.

METHOD DETAILS

Electrode assembly—Microelectrodes consisted of a drivable bundle of sixteen 25.4 μm diameter Formvar-Insulated Nichrome wires (761500, A-M Systems, Carlsborg, WA) within a 27-gauge cannula (B000FN3M7K, Amazon Supply) and two 127 μm diameter PFA-coated, annealed strength stainless-steel ground wires (791400, A-M Systems, Carlsborg, WA). All wires were electrically connected to a nano-strip Omnetics connector (A79042-001, Omnetics Connector Corp., Minneapolis, MN) on a custom 24-contact, individually routed and gold immersed circuit board (San Francisco Circuits, San Mateo, CA). Sixteen individual recording wires were soldered to individual channels of an

Omnetics connector. The sixteen wire bundle was integrated into a microdrive permitting advancement in ~40 μm increments.

Surgery—Stereotaxic surgery was performed aseptic conditions under isoflurane anesthesia (1-5% in oxygen). Carprofen (5 mg/kg, s.c.) and lactated ringer's solution (10 Ml, s.c.) were administered preoperatively. The skull was scoured in a crosshatch pattern with a scalpel blade to increase efficacy of implant adhesion. Six screws were installed in the skull to further stabilize the connection between the skull, electrode assembly and a protective head cap. A 1.4 mm diameter craniotomy was performed to remove a circular skull section centered on the implant site and the underlying dura was removed to expose the cortex. Nichrome recording wires were freshly cut with surgical scissors to extend ~2.0 mm beyond the cannula. Just before implant, current was delivered to each recording wire in a saline bath, stripping each tip of its formvar insulation. Current was supplied by a 12V lantern battery and each Omnetics connector contact was stimulated for 2s using a lead. Machine grease was placed by the cannula and on the microdrive.

For implantation dorsal to the RRF, the electrode assembly was slowly advanced to the following coordinates from cortex (anterior-posterior: −7.15 mm, medial-lateral: −1.35 mm and dorsal-ventral: −5.9 mm). Once in place, stripped ends of both ground wires were wrapped around two screws to ground the electrode. The microdrive base and a protective head cap surrounding the electrode assembly were cemented in place at the end of the procedure using orthodontic resin (C 22-05-98, Pearson Dental Supply, Sylmar, CA), and the Omnetics connector was affixed to the head cap.

Behavior apparatus—The apparatus for Pavlovian fear discrimination consisted of two individual chambers with aluminum front and back walls retrofitted with clear plastic covers, clear acrylic sides and top, and a grid floor. Each grid floor bar was electrically connected to an aversive shock generator (Med Associates, St. Albans, VT) through a grounding device. This permitted the floor to be grounded at all times except during shock delivery. An external food cup and a central nose poke opening, equipped with infrared photocells were present on one wall. Auditory stimuli were presented through two speakers mounted on the ceiling. Behavior chambers were modified to allow for free movement of the electrophysiology cable during behavior; plastic funnels were epoxied to the top of the behavior chambers with the larger end facing down, and the tops of the chambers were cut to the opening of the funnel.

Nose poke acquisition—Prior to discrimination sessions, rats were food deprived to 85% of their free-feeding body weight and were fed specifically to maintain this weight through the behavioral procedure. Rats were shaped to nose poke for pellet (Bio-Serv, Flemington, NJ) delivery in the experimental chamber using a fixed ratio schedule in which one nose poke yielded one pellet. Shaping sessions lasted 30 min or until approximately 50 nose pokes were completed. Over the next 5 days, rats were placed on variable interval (VI) schedules in which nose pokes were reinforced on average every 30 s (VI-30, day 1), or 60 s (days 2 through 5). For the remainder of behavioral testing, nose pokes were reinforced on a VI-60 schedule independent of all Pavlovian contingencies.

Fear discrimination—Prior to recording, each rat received eight sessions of fear discrimination. Each session consisted of 16 trials, with a mean inter-trial interval of 3.5 min. Auditory cues were 10 s in duration and consisted of repeating motifs of a broadband click, phaser, or trumpet (listen or download: http://mcdannaldlab.org/resources/ardbark). Each cue was associated with a unique probability of foot shock (0.5 mA, 0.5 s): danger, $p = 1.00$; uncertainty, $p = 0.25$; and safety, $p = 0.00$. Auditory identity was counterbalanced across rats. Foot shock was administered 2 s following the termination of the auditory cue on danger and uncertainty shock trials. This was done in order to observe possible neural activity during the delay period not driven by an explicit cue. A single session consisted of four danger trials, two uncertainty shock trials, six uncertainty omission trials, and four safety trials. The order of trial type presentation was randomly determined by the behavioral program, and differed for each rat, each session. After the eighth session, rats were removed from discrimination, given full food and received stereotaxic surgery. Following recovery, discrimination resumed with single-unit recording. The microelectrode bundles were advanced in ~80 μm steps every other day to record from new units during the following session.

Single-unit data acquisition—During recording sessions, a 1x amplifying headstage connected the Omnetics connector to the commutator via a shielded recording cable (Headstage: 40684-020 & Cable: 91809-017, Plexon Inc., Dallas TX). Analog neural activity was digitized and high-pass filtered via amplifier to remove low-frequency artifacts and sent to the Ominplex D acquisition system (Plexon Inc., Dallas TX). Behavioral events (cues, shocks, nose pokes) were controlled and recorded by a computer running Med Associates software. Timestamped events from Med Associates were sent to Ominplex D acquisition system via a dedicated interface module (DIG-716B). The result was a single file (.pl2) containing all time stamps for recording and behavior. Single units were sorted offline with a template-based spike-sorting algorithm (Offline Sorter V3 Plexon Inc., Dallas TX). Timestamped spikes and events (cues, shocks, nose pokes) were extracted and analyzed with statistical routines in Matlab (Natick, MA).

Histology—Rats were deeply anesthetized using isoflurane and final electrode coordinates were marked by passing current from a 6V battery through 4 of the 16 nichrome electrode wires. Rats were perfused with 0.9% biological saline and 4% paraformaldehyde in a 0.2 M Potassium Phosphate Buffered Solution. Brains were extracted and postfixed in a 10% neutral-buffered formalin solution for 24 h, stored in 10% sucrose/formalin and sectioned via microtome. All brains processed for light microscopy using anti-tyrosine hydroxylase immunohistochemistry (AB152, Millipore-Sigma) and a NovaRed chromagen reaction (SK-4800, Vector Laboratories, Burlingame, CA). Sections were mounted, imaged using a light microscope (Axio Imager Z2, Zeiss, Thornwood, NY) and electrode placement was confirmed[94].

Verifying electrode placement—Passing current through the wire permitted the tip locations to be observed in brain sections. In addition, wire tracks leading up to tips were visible. Starting with the electrode tips, the driving path of the electrode through the brain was backwards calculated. Only single units originating from anterior-posterior and dorsal-

ventral locations that included tyrosine hydroxylase staining of A8 dopamine neurons were considered for analysis (Figure 1C and D). Data from rats with incorrect electrode placement (n = 3) were excluded from further analyses.

QUANTIFICATION AND STATISTICAL ANALYSIS

Calculating suppression ratios—Fear was measured by suppression of rewarded nose poking, calculated as a ratio: [(baseline poke rate − cue poke rate) / (baseline poke rate + cue poke rate)]. The baseline nose poke rate was taken from the 20 s prior to cue onset and the cue poke rate from the 10 s cue period. Suppression ratios were calculated for each trial using only that trial's baseline. A ratio of '1' indicated high fear, '0' low fear, and gradations between intermediate levels of fear. The distribution of suppression ratios was visualized using the plotSpread function for Matlab (https://www.mathworks.com/matlabcentral/fileexchange/37105-plot-spread-points-beeswarm-plot).

95% Bootstrap confidence intervals—95% bootstrap confidence intervals were constructed for differential firing, beta coefficients and suppression ratios using the bootci function in Matlab. For each bootstrap, a distribution was created by sampling the data 1,000 times with replacement. Studentized confidence intervals were constructed with the final outputs being the mean, lower bound and upper bound of the 95% bootstrap confidence interval. 95% confidence intervals were used to determine if differential firing, beta coefficients and suppression ratios were observed. 95% bootstrap confidence intervals containing zero support the null hypothesis that differential firing, beta coefficients and suppression ratios were not observed. 95% bootstrap confidence intervals that do not contain zero reject the null hypothesis, and support the interpretation that differential firing, beta coefficients and suppression ratios were observed.

Identifying cue-responsive neurons—Single units were screened for cue responsiveness by comparing raw firing rate (Hz) during the 10-s period just prior to cue onset (baseline), to mean firing rate (Hz) during the first 1-s cue interval and the final 5-s cue interval. A neuron was considered cue-responsive if it showed a significant change in firing from baseline (increase or decrease; paired, two-tailed t-test, $p < 0.05$) to danger, uncertainty or safety during the first 1-s or the last 5-s interval. Bonferroni correction (0.5/6) was not performed because this criterion was too stringent, resulting in many obviously cue-responsive neurons being omitted from analysis.

K-means clustering—Clustering was performed using the Matlab kmeans function. Firing rate of all cue-responsive neurons (n = 423) was summarized in a 423 neuron x 54 epoch matrix. The 54 epochs were taken from the 10, 1-s cue intervals (danger, epochs 1-10; uncertainty, epochs 11-20; and safety, epochs 21-30) and from 6, 1-s intervals following shock and omission (danger, epochs 31-36; uncertainty shock, epochs 37-42; uncertainty omission, epochs 43-48; and safety, epochs 49-54). Clustering was performed 10 times, incrementing from 1 to 15 clusters. The result was the cluster identity for each neuron and the mean of the squared Euclidean distance between each point and its cluster centroid (Figure 1E).

Heat plot and color maps—Heat plots were constructed from normalized firing rate using the imagesc function in Matlab. Perceptually uniform color maps were used to prevent visual distortion of the data[95].

Firing and waveform characteristics—The following characteristics were determined for each cue-responsive neuron: baseline firing rate, coefficient of variance, coefficient of skewness, waveform half duration, and waveform amplitude ratio. Baseline firing rate was mean firing rate (Hz) during the 10 s prior to cue onset. Inter-spike intervals were calculated for the 20 s prior to cue onset for each of the 16 trials. Coefficient of variance was calculated by $[(SD_{ISI} / \overline{X}_{ISI}]$, in which SD_{ISI} was the standard deviation of inter-spike interval, and $\overline{X}_{ISI}$ was the mean inter-spike interval. Coefficient of variance is a relative measure of the variability of spike firing, with small values indicating less variation in inter-spike intervals (more regular firing), and large values more variability (less regular firing)[96,97]. Coefficient of skewness was calculated by $[(3 \times (\overline{X}_{ISI} - \widetilde{X}_{ISI})) / SD_{ISI}]$, in which $\overline{X}_{ISI}$, $\widetilde{X}_{ISI}$, and SD_{ISI} were the mean, median and standard deviation of inter-spike interval, respectively. Coefficient of skewness is a measure of the asymmetry of the distribution of the inter-spike intervals, with positive values indicating longer intervals (less regular firing) and negative values indicating shorter intervals (more regular firing)[96]. Waveform amplitude ratio was calculated by [(N−P)/(N+P)], in which P was the y-axis distance between the initial value and peak initial hyperpolarization, and N was the y-axis distance between the peak initial value and valley of depolarization. Values near zero indicate a relatively large initial hyper-polarization while values near one indicate a relatively small initial hyperpolarization[12,74]. Waveform half duration was calculated by [D/2)], in which D was the x-axis distance between the valley of depolarization and the peak of after-hyperpolarization and smaller values indicate narrower waveforms[12,74].

Z-score normalization—For each neuron, and for each trial type, firing rate (Hz) was calculated in 250 ms bins from 20 s prior to cue onset to 20 s following cue offset, for a total of 200 bins. Mean firing rate over the 200 bins was calculated by averaging all trials for each trial type. Mean differential firing rate was calculated for each of the 200 bins by subtracting mean baseline firing rate (2-s prior to cue onset), specific to that trial type, from each bin. Mean differential firing was Z-score normalized across all trial types within a single neuron, such that mean firing = 0, and standard deviation in firing = 1. Z-score normalization was applied to firing across the entirety of the recording epoch, as opposed to only the baseline period, in case neurons showed little/no baseline activity. As a result, periods of phasic, excitatory and inhibitory firing contributed to normalized mean firing rate (0). For this reason, Z-score normalized baseline activity can differ from zero. Z-score normalized firing was analyzed with ANOVA using group, bin and trial type as factors. F and *p*-values (*p*) are reported, as well as partial eta squared (ηp^2) and observed power (op).

Population and single-unit firing analyses—Population firing for each trial types (danger, uncertainty and safety) was analyzed using ANOVA with cluster, trial type and interval (250 ms bins) as factors (Figure 3). Uncertainty trial types were collapsed because they did not differ for either suppression ratio or firing analysis. This was expected, during cue presentation rats did not know the current uncertainty trial type. F statistic, *p*-value (*p*),

partial eta squared (ηp^2) and observed power (op) are reported for main effects and interactions. Differential firing to each cue between the groups was compared using independent sample t-test, corrected for three comparisons. Within-neuron, cue firing relationships were determined by calculating the R^2 and *p*-value (*p*) for the Pearson's correlation coefficient. Population firing during the post shock period was smoothed using Savitzky-Golay filtering in Matlab (sgolayfilt function). Smoothing was for visualization only, all analyses were performed on unsmoothed normalized firing rate. Fisher r-to-z transformation for dependent samples was performed with Meng's Z-test for correlated correlation coefficients: (https://www.mathworks.com/matlabcentral/fileexchange/37867-meng-s-z-test-for-correlated-correlation-coefficients).

Single-unit, linear regression—Single-unit, linear regression was used to determine the degree to which fear output and/or threat probability explained trial-by-trial variation in firing of single neurons in a specific time interval. For each regression, all 16 trials from a single session were ordered by type. Z-score normalized firing rate was specified for the interval of interest. The fear output regressor was the suppression ratio for the entire cue, for that specific trial. The threat probability regressor was the foot shock probability associated with the specific cue. Regression (using the regress function in Matlab) required a separate, constant input. The regression output of greatest interest was the beta coefficient for each regressor (fear output and threat probability), quantifying the strength (greater distance from zero = stronger) and direction (>0 = positive) of the predictive relationship between each regressor and single-unit firing. ANOVA was used to analyze beta coefficients, exactly as described for normalized firing rate.

Threat probability tuning curve—Nine separate regression analyses were performed as above. Only now, the value assigned to uncertainty component of the threat probability regressor was systematically increased from 0 to 1 in 0.125 steps (0.000, 0.125, 0.250, 0.025, 0.500, 0.625, 0.750, 0.875, and 1.000). The first regression used the value of 0.000, second regression 0.125 and so on. Regression was performed for each 1-s bin of the 10-s cue. Beta coefficients for all 10 bins were averaged to produce a single threat tuning curve. Percent of peak beta coefficient (threat probability) value was calculated by dividing the mean of each uncertainty interval by the mean of the peak interval.

ADDITIONAL RESOURCES

Med Associates programs used for behavior and Matlab programs used for behavioral analyses are made freely available at our lab website: http://mcdannaldlab.org/resources

Supplementary Material

Refer to Web version on PubMed Central for supplementary material.

ACKNOWLEDGEMENTS

We thank Bret Judson and the Boston College Imaging Core for infrastructure and support. Research reported in this publication was supported by the National Institute of Mental Health of the National Institutes of Health under Award Numbers MH113053 and MH117791. The content is solely the responsibility of the authors and does not

necessarily represent the official views of the National Institutes of Health. The authors report no competing interests.

REFERENCES

1. Hitchcock J, and Davis M (1986). Lesions of the amygdala, but not of the cerebellum or red nucleus, block conditioned fear as measured with the potentiated startle paradigm. Behav Neurosci 100, 11–22. [PubMed: 3954873]
2. Kapp BS, Frysinger RC, Gallagher M, and Haselton JR (1979). Amygdala central nucleus lesions: effect on heart rate conditioning in the rabbit. Physiol Behav 23, 1109–17. [PubMed: 542522]
3. Gallagher M, Kapp BS, Musty RE, and Driscoll PA (1977). Memory formation: evidence for a specific neurochemical system in the amygdala. Science 198, 423–5. [PubMed: 20664]
4. LeDoux JE, Iwata J, Cicchetti P, and Reis DJ (1988). Different projections of the central amygdaloid nucleus mediate autonomic and behavioral correlates of conditioned fear. Journal of Neuroscience 8, 2517–29. [PubMed: 2854842]
5. Ressler RL, and Maren S (2019). Synaptic encoding of fear memories in the amygdala. Curr Opin Neurobiol 54, 54–59. [PubMed: 30216780]
6. Tovote P, Fadok JP, and Luthi A (2015). Neuronal circuits for fear and anxiety. Nat Rev Neurosci 16, 317–31. [PubMed: 25991441]
7. Davis P, and Reijmers LG (2018). The dynamic nature of fear engrams in the basolateral amygdala. Brain Res Bull 141, 44–49. [PubMed: 29269319]
8. Sonerud GA (1985). Nest Hole Shift in Tengmalms Owl Aegolius-Funereus as Defense against Nest Predation Involving Long-Term-Memory in the Predator. J Anim Ecol 54, 179–192.
9. Tjaden PG, Thoennes N, National Institute of Justice (U. S.), and Centers for Disease Control and Prevention (U. S.) (2000). Full report of the prevalence, incidence, and consequences of violence against women : findings from the National Violence Against Women Survey (U.S. Department of Justice, Office of Justice Programs, National Insitute of Justice).
10. Vetere G, Kenney JW, Tran LM, Xia F, Steadman PE, Parkinson J, Josselyn SA, and Frankland PW (2017). Chemogenetic Interrogation of a Brain-wide Fear Memory Network in Mice. Neuron 94, 363–374 e4. [PubMed: 28426969]
11. Beck CH, and Fibiger HC (1995). Conditioned fear-induced changes in behavior and in the expression of the immediate early gene c-fos: with and without diazepam pretreatment. Journal of Neuroscience 15, 709–20. [PubMed: 7823174]
12. Wright KM, and McDannald MA (2019). Ventrolateral periaqueductal gray neurons prioritize threat probability over fear output. Elife 8.
13. Mobbs D, Yu RJ, Rowe JB, Eich H, FeldmanHall O, and Dalgleish T (2010). Neural activity associated with monitoring the oscillating threat value of a tarantula. P Natl Acad Sci USA 107, 20582–20586.
14. McNally GP, Johansen JP, and Blair HT (2011). Placing prediction into the fear circuit. Trends in neurosciences 34, 283–92. [PubMed: 21549434]
15. Walker RA, Wright KM, Jhou TC, and McDannald MA (2019). The ventrolateral periaqueductal grey updates fear via positive prediction error. Eur. J. Neurosci
16. McHugh SB, Barkus C, Huber A, Capitao L, Lima J, Lowry JP, and Bannerman DM (2014). Aversive prediction error signals in the amygdala. The Journal of neuroscience: the official journal of the Society for Neuroscience 34, 9024–33. [PubMed: 24990922]
17. Roy M, Shohamy D, Daw N, Jepma M, Wimmer GE, and Wager TD (2014). Representation of aversive prediction errors in the human periaqueductal gray. Nature neuroscience 17, 1607–12. [PubMed: 25282614]
18. Groessl F, Munsch T, Meis S, Griessner J, Kaczanowska J, Pliota P, Kargl D, Badurek S, Kraitsy K, Rassoulpour A, et al. (2018). Dorsal tegmental dopamine neurons gate associative learning of fear. Nat Neurosci 21, 952–962. [PubMed: 29950668]
19. Jimenez-Castellanos J, and Graybiel AM (1987). Subdivisions of the dopamine-containing A8-A9-A10 complex identified by their differential mesostriatal innervation of striosomes and extrastriosomal matrix. Neuroscience 23, 223–42. [PubMed: 3683862]

20. Stratford TR, and Wirtshafter D (1990). Ascending dopaminergic projections from the dorsal raphe nucleus in the rat. Brain Res 511, 173–6. [PubMed: 1970510]
21. Herbert H (1992). Evidence for Projections from Medullary Nuclei onto Serotonergic and Dopaminergic-Neurons in the Midbrain Dorsal Raphe Nucleus of the Rat. Cell Tissue Res 270, 149–156. [PubMed: 1358454]
22. Williams SM, and Goldman-Rakic PS (1998). Widespread origin of the primate mesofrontal dopamine system. Cereb Cortex 8, 321–345. [PubMed: 9651129]
23. Prasad K, and Richfield EK (2010). Number and nuclear morphology of TH+ and TH− neurons in the mouse ventral midbrain using epifluorescence stereology. Exp Neurol 225, 328–340. [PubMed: 20637754]
24. Nair-Roberts RG, Chatelain-Badie SD, Benson E, White-Cooper H, Bolam JP, and Ungless MA (2008). Stereological estimates of dopaminergic, GABAergic and glutamatergic neurons in the ventral tegmental area, substantia nigra and retrorubral field in the rat. Neuroscience 152, 1024–31. [PubMed: 18355970]
25. Morales M, and Root DH (2014). Glutamate neurons within the midbrain dopamine regions. Neuroscience 282C, 60–68.
26. Yamaguchi T, Wang HL, and Morales M (2013). Glutamate neurons in the substantia nigra compacta and retrorubral field. Eur J Neurosci 38, 3602–10. [PubMed: 24102658]
27. van Zessen R, Phillips JL, Budygin EA, and Stuber GD (2012). Activation of VTA GABA Neurons Disrupts Reward Consumption. Neuron 73, 1184–1194. [PubMed: 22445345]
28. Qi J, Zhang S, Wang HL, Barker DJ, Miranda-Barrientos J, and Morales M (2016). VTA glutamatergic inputs to nucleus accumbens drive aversion by acting on GABAergic interneurons. Nat Neurosci 19, 725–733. [PubMed: 27019014]
29. Vonkrosigk M, and Smith AD (1991). Descending Projections from the Substantia-Nigra and Retrorubral Field to the Medullary and Pontomedullary Reticular-Formation. Eur J Neurosci 3, 260–273. [PubMed: 12106204]
30. Ray MH, Russ AN, Walker RA, and McDannald MA (2020). The Nucleus Accumbens Core is Necessary to Scale Fear to Degree of Threat. J. Neurosci, JN-RM-0299-20.
31. Thomas KL, Hall J, and Everitt BJ (2002). Cellular imaging with zif268 expression in the rat nucleus accumbens and frontal cortex further dissociates the neural pathways activated following the retrieval of contextual and cued fear memory. European Journal of Neuroscience 16, 1789–96.
32. Moaddab M, Ray MH, and McDannald MA (2021). Ventral pallidum neurons dynamically signal relative threat. Communications Biology 4, 1–14. [PubMed: 33398033]
33. Stephenson-Jones M, Bravo-Rivera C, Ahrens S, Furlan A, Xiao X, Fernandes-Henriques C, and Li B (2020). Opposing Contributions of GABAergic and Glutamatergic Ventral Pallidal Neurons to Motivational Behaviors. Neuron 105, 921–933.e5. [PubMed: 31948733]
34. Goode TD, and Maren S (2017). Role of the bed nucleus of the stria terminalis in aversive learning and memory. Learn. Mem 24, 480–491. [PubMed: 28814474]
35. Walker DL, Toufexis DJ, and Davis M (2003). Role of the bed nucleus of the stria terminalis versus the amygdala in fear, stress, and anxiety. European Journal of Pharmacology 463, 199–216. [PubMed: 12600711]
36. Deutch AY, Goldstein M, Baldino F Jr., and Roth RH (1988). Telencephalic projections of the A8 dopamine cell group. Ann N Y Acad Sci 537, 27–50. [PubMed: 2462395]
37. Gasbarri A, Packard MG, Sulli A, Pacitti C, Innocenzi R, and Perciavalle V (1996). The projections of the retrorubral field A8 to the hippocampal formation in the rat. Exp Brain Res 112, 244–252. [PubMed: 8951393]
38. Yu K, Ahrens S, Zhang X, Schiff H, Ramakrishnan C, Fenno L, Deisseroth K, Zhao F, Luo M-H, Gong L, et al. (2017). The central amygdala controls learning in the lateral amygdala. Nature Neuroscience 20, 1680–1685. [PubMed: 29184202]
39. Zahm DS (2008). The dopaminergic projection system, basal forebrain macrosystems, and conditioned stimuli. CNS Spectr 13, 32–40. [PubMed: 18204412]
40. Walker RA, Andreansky C, Ray MH, and McDannald MA (2018). Early adolescent adversity inflates threat estimation in females and promotes alcohol use initiation in both sexes. Behav. Neurosci 132, 171–182. [PubMed: 29809045]

41. Ray MH, Hanlon E, and McDannald MA (2018). Lateral orbitofrontal cortex partitions mechanisms for fear regulation and alcohol consumption. PLoS ONE 13, e0198043. [PubMed: 29856796]
42. Wright KM, DiLeo A, and McDannald MA (2015). Early adversity disrupts the adult use of aversive prediction errors to reduce fear in uncertainty. Front Behav Neurosci 9, 227. [PubMed: 26379520]
43. Berg BA, Schoenbaum G, and McDannald MA (2014). The dorsal raphe nucleus is integral to negative prediction errors in Pavlovian fear. European Journal of Neuroscience 40, 3096–3101.
44. Pickens CL, Golden SA, Adams-Deutsch T, Nair SG, and Shaham Y (2009). Long-lasting incubation of conditioned fear in rats. Biological Psychiatry 65, 881–6. [PubMed: 19167702]
45. Anglada-Figueroa D, and Quirk GJ (2005). Lesions of the basal amygdala block expression of conditioned fear but not extinction. Journal of Neuroscience 25, 9680–5. [PubMed: 16237172]
46. Annau Z, and Kamin LJ (1961). The conditioned emotional response as a function of intensity of the US. Journal of Comparative and Physiological Psychology 54, 428–432. [PubMed: 13683658]
47. Rescorla RA (1968). Probability of shock in the presence and absence of CS in fear conditioning. Journal of Comparative and Physiological Psychology 66, 1–5. [PubMed: 5672628]
48. Bouton ME, and Bolles RC (1980). Conditioned fear assessed by freezing and by the suppression of three different baselines. Animal Learning & Behavior 8, 429–434.
49. Ungless MA, and Grace AA (2012). Are you or aren't you? Challenges associated with physiologically identifying dopamine neurons. Trends Neurosci 35, 422–430. [PubMed: 22459161]
50. Eshel N, Bukwich M, Rao V, Hemmelder V, Tian J, and Uchida N (2015). Arithmetic and local circuitry underlying dopamine prediction errors. Nature 525, 243–6. [PubMed: 26322583]
51. Cohen JY, Haesler S, Vong L, Lowell BB, and Uchida N (2012). Neuron-type-specific signals for reward and punishment in the ventral tegmental area. Nature 482, 85–8. [PubMed: 22258508]
52. Sadacca BF, Jones JL, and Schoenbaum G (2016). Midbrain dopamine neurons compute inferred and cached value prediction errors in a common framework. Elife 5.
53. Salinas-Hernandez XI, Vogel P, Betz S, Kalisch R, Sigurdsson T, and Duvarci S (2018). Dopamine neurons drive fear extinction learning by signaling the omission of expected aversive outcomes. Elife 7.
54. Luo R, Uematsu A, Weitemier A, Aquili L, Koivumaa J, McHugh TJ, and Johansen JP (2018). A dopaminergic switch for fear to safety transitions. Nat Commun 9.
55. Yan R, Wang T, and Zhou Q (2019). Elevated dopamine signaling from ventral tegmental area to prefrontal cortical parvalbumin neurons drives conditioned inhibition. PNAS 116, 13077–13086. [PubMed: 31182594]
56. Wenzel JM, Oleson EB, Gove WN, Cole AB, Gyawali U, Dantrassy HM, Bluett RJ, Dryanovski DI, Stuber GD, Deisseroth K, et al. (2018). Phasic Dopamine Signals in the Nucleus Accumbens that Cause Active Avoidance Require Endocannabinoid Mobilization in the Midbrain. Curr Biol 28, 1392–1404 e5. [PubMed: 29681476]
57. Mileykovskiy B, and Morales M (2011). Duration of Inhibition of Ventral Tegmental Area Dopamine Neurons Encodes a Level of Conditioned Fear. J. Neurosci 31, 7471–7476. [PubMed: 21593330]
58. Fadok JP, Dickerson TMK, and Palmiter RD (2009). Dopamine Is Necessary for Cue-Dependent Fear Conditioning. J. Neurosci 29, 11089–11097. [PubMed: 19741115]
59. Jo YS, Heymann G, and Zweifel LS (2018). Dopamine Neurons Reflect the Uncertainty in Fear Generalization. Neuron 100, 916–+. [PubMed: 30318411]
60. Parker JG, Wanat MJ, Soden ME, Ahmad K, Zweifel LS, Bamford NS, and Palmiter RD (2011). Attenuating GABAA Receptor Signaling in Dopamine Neurons Selectively Enhances Reward Learning and Alters Risk Preference in Mice. J. Neurosci 31, 17103–17112. [PubMed: 22114279]
61. Maes EJ, Sharpe MJ, Usypchuk AA, Lozzi M, Chang CY, Gardner MPH, Schoenbaum G, and Iordanova MD (2020). Causal evidence supporting the proposal that dopamine transients function as temporal difference prediction errors. Nat Neurosci 23, 176–178. [PubMed: 31959935]

62. Sharpe MJ, Batchelor HM, Mueller LE, Yun Chang C, Maes EJP, Niv Y, and Schoenbaum G (2020). Dopamine transients do not act as model-free prediction errors during associative learning. Nat Commun 11.
63. Menegas W, Akiti K, Amo R, Uchida N, and Watabe-Uchida M (2018). Dopamine neurons projecting to the posterior striatum reinforce avoidance of threatening stimuli. Nat Neurosci 21, 1421–1430. [PubMed: 30177795]
64. de Jong JW, Afjei SA, Dorocic IP, Peck JR, Liu C, Kim CK, Tian L, Deisseroth K, and Lammel S (2019). A Neural Circuit Mechanism for Encoding Aversive Stimuli in the Mesolimbic Dopamine System. Neuron 101, 133–+. [PubMed: 30503173]
65. Lammel S, Lim BK, and Malenka RC (2014). Reward and aversion in a heterogeneous midbrain dopamine system. Neuropharmacology 76 Pt B, 351–9. [PubMed: 23578393]
66. Zhou Z, Liu XM, Chen SP, Zhang ZJ, Liu YM, Montardy Q, Tang YQ, Wei PF, Liu N, Li L, et al. (2019). A VTA GABAergic Neural Circuit Mediates Visually Evoked Innate Defensive Responses. Neuron 103, 473-+. [PubMed: 31202540]
67. Engelhard B, Finkelstein J, Cox J, Fleming W, Jang HJ, Ornelas S, Koay SA, Thiberge SY, Daw ND, Tank DW, et al. (2019). Specialized coding of sensory, motor and cognitive variables in VTA dopamine neurons. Nature 570, 509–+. [PubMed: 31142844]
68. Eichenbaum H (2014). Time cells in the hippocampus: a new dimension for mapping memories. Nat Rev Neurosci 15, 732–44. [PubMed: 25269553]
69. MacDonald CJ, Carrow S, Place R, and Eichenbaum H (2013). Distinct Hippocampal Time Cell Sequences Represent Odor Memories in Immobilized Rats. J Neurosci 33, 14607–14616. [PubMed: 24005311]
70. Kraus BJ, Robinson RJ, White JA, Eichenbaum H, and Hasselmo ME (2013). Hippocampal “Time Cells”: Time versus Path Integration. Neuron 78, 1090–1101. [PubMed: 23707613]
71. Zhou J, Montesinos-Cartagena M, Wikenheiser AM, Gardner MPH, Niv Y, and Schoenbaum G (2019). Complementary Task Structure Representations in Hippocampus and Orbitofrontal Cortex during an Odor Sequence Task. Curr. Biol 29, 3402–3409.e3. [PubMed: 31588004]
72. Kennedy A, Kunwar PS, Li L, Stagkourakis S, Wagenaar DA, and Anderson DJ (2020). Stimulus-specific hypothalamic encoding of a persistent defensive state. Nature 586, 730–734. [PubMed: 32939094]
73. Takahashi YK, Batchelor HM, Liu B, Khanna A, Morales M, and Schoenbaum G (2017). Dopamine Neurons Respond to Errors in the Prediction of Sensory Features of Expected Rewards. Neuron 95, 1395–1405 e3. [PubMed: 28910622]
74. Roesch MR, Calu DJ, and Schoenbaum G (2007). Dopamine neurons encode the better option in rats deciding between differently delayed or sized rewards. Nature Neuroscience 10, 1615–24. [PubMed: 18026098]
75. Schultz W, Dayan P, and Montague PR (1997). A neural substrate of prediction and reward. Science 275, 1593–9. [PubMed: 9054347]
76. Glimcher PW, Mullette-Gillman OA, Bayer HM, Lau B, and Rutledge R (2005). Dopamine encodes a quantiative reward prediction error for for reinforcement learning. Neuropsychopharmacol 30, S27–S27.
77. Vianna DML, and Carrive P (2005). Changes in cutaneous and body temperature during and after conditioned fear to context in the rat. Eur J Neurosci 21, 2505–2512. [PubMed: 15932607]
78. Carrive P (2000). Conditioned fear to environmental context: cardiovascular and behavioral components in the rat. Brain Research 858, 440–445. [PubMed: 10708699]
79. Kim EJ, Kong M-S, Park SG, Mizumori SJY, Cho J, and Kim JJ (2018). Dynamic coding of predatory information between the prelimbic cortex and lateral amygdala in foraging rats. Sci Adv 4, eaar7328. [PubMed: 29675471]
80. Rozeske RR, Jercog D, Karalis N, Chaudun F, Khoder S, Girard D, Winke N, and Herry C (2018). Prefrontal-Periaqueductal Gray-Projecting Neurons Mediate Context Fear Discrimination. Neuron 97, 898–910 e6. [PubMed: 29398355]
81. Sarlitto MC, Foilb AR, and Christianson JP (2018). Inactivation of the Ventrolateral Orbitofrontal Cortex Impairs Flexible Use of Safety Signals. Neuroscience 379, 350–358. [PubMed: 29604383]

82. Ozawa T, Ycu EA, Kumar A, Yeh LF, Ahmed T, Koivumaa J, and Johansen JP (2017). A feedback neural circuit for calibrating aversive memory strength. Nat Neurosci 20, 90–97. [PubMed: 27842071]
83. Iordanova MD, McNally GP, and Westbrook RF (2006). Opioid receptors in the nucleus accumbens regulate attentional learning in the blocking paradigm. J Neurosci 26, 4036–4045. [PubMed: 16611820]
84. Iordanova MD (2009). Dopaminergic Modulation of Appetitive and Aversive Predictive Learning. Rev Neuroscience 20, 383–404.
85. Li SSY, and McNally GP (2015). A Role of Nucleus Accumbens Dopamine Receptors in the Nucleus Accumbens Core, but Not Shell, in Fear Prediction Error. Behav Neurosci 129, 450–456. [PubMed: 26098230]
86. Oleson EB, Gentry RN, Chioma VC, and Cheer JF (2012). Subsecond dopamine release in the nucleus accumbens predicts conditioned punishment and its successful avoidance. J Neurosci 32, 14804–8. [PubMed: 23077064]
87. Abraham AD, Neve KA, and Lattal KM (2016). Activation of D1/5 Dopamine Receptors: A Common Mechanism for Enhancing Extinction of Fear and Reward-Seeking Behaviors. Neuropsychopharmacology 41, 2072–81. [PubMed: 26763483]
88. Nader K, and LeDoux J (1999). The dopaminergic modulation of fear: quinpirole impairs the recall of emotional memories in rats. Behav Neurosci 113, 152–65. [PubMed: 10197915]
89. Nader K, and LeDoux JE (1999). Inhibition of the mesoamygdala dopaminergic pathway impairs the retrieval of conditioned fear associations. Behav Neurosci 113, 891–901. [PubMed: 10571473]
90. Badrinarayan A, Wescott SA, Vander Weele CM, Saunders BT, Couturier BE, Maren S, and Aragona BJ (2012). Aversive Stimuli Differentially Modulate Real-Time Dopamine Transmission Dynamics within the Nucleus Accumbens Core and Shell. J Neurosci 32, 15779–15790. [PubMed: 23136417]
91. Guarraci FA, and Kapp BS (1999). An electrophysiological characterization of ventral tegmental area dopaminergic neurons during differential pavlovian fear conditioning in the awake rabbit. Behavioural brain research 99, 169–79. [PubMed: 10512583]
92. Gore BB, Soden ME, and Zweifel LS (2014). Visualization of plasticity in fear-evoked calcium signals in midbrain dopamine neurons. Learn Mem 21, 575–9. [PubMed: 25320348]
93. Tiklová K, Björklund å.K., Lahti L, Fiorenzano A, Nolbrant S, Gillberg L, Volakakis N, Yokota C, Hilscher MM, Hauling T, et al. (2019). Single-cell RNA sequencing reveals midbrain dopamine neuron diversity emerging during mouse brain development. Nature Communications 10, 581.
94. Paxinos G, and Watson C (2007). The rat brain in stereotaxic coordinates 6th ed. (Academic Press/ Elsevier).
95. Crameri F (2018). Scientific colour maps (Version 4.0.0).
96. Saeb-Parsy K, and Dyball REJ (2003). Defined Cell Groups in the Rat Suprachiasmatic Nucleus Have Different Day/Night Rhythms of Single-Unit Activity In Vivo. J Biol Rhythms 18, 26–42. [PubMed: 12568242]
97. Moaddab M, Hyland BI, and Brown CH (2015). Oxytocin excites nucleus accumbens shell neurons in vivo. Molecular and Cellular Neuroscience 68, 323–330. [PubMed: 26343002]

Highlights

- Rats fully discriminate cues for danger, uncertainty and safety
- RRF neurons bias firing towards danger and uncertainty cues
- Substantial diversity in the pattern, timing, direction and magnitude of cue firing
- RRF firing diversity extends to aversive outcome

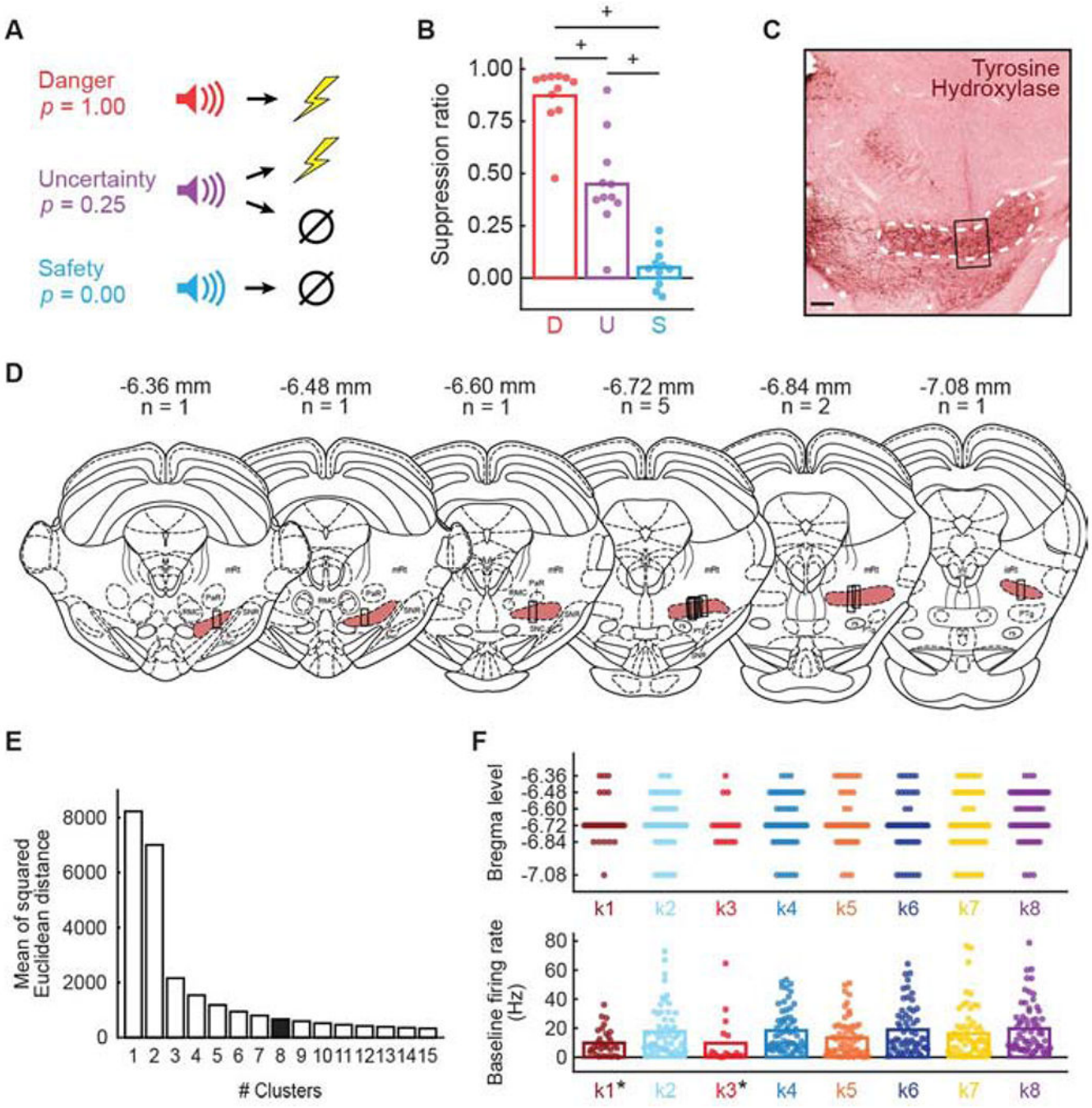

Figure 1. Fear discrimination, behavior, histology and firing characteristics

(**A**) Auditory cues predicted unique foot shock probabilities: danger ($p = 1.00$), uncertainty ($p = 0.25$), and safety ($p = 0.00$). (**B**) Mean (bar) and individual (data points) suppression ratio for each cue (D, danger, red; U, uncertainty, purple; S, safety, blue) is shown for all sessions with cue-responsive neurons for all rats (n = 11). $^{+}$95% bootstrap confidence interval for differential suppression ratio does not contain zero. (**C**) Example of electrode placement is visualized with tyrosine hydroxylase immunohistochemistry. White dashed line indicates A8 boundary; black rectangle indicates region from which single units were

obtained. Scale bar = 50 μm. (**D**) Histological reconstruction of microelectrode bundle placements are represented by black bars from anterior to the posterior RRF (shown in rouge), bregma levels and number of animals indicated. Mesencephalic reticular formation (*m*Rt), pararubral nucleus (PaR), red nucleus magnocellular part (RMC), substantia nigra pars reticulata (SNR), substantia nigra pars compacta (SNC), pedunculopontine tegmental (PTg), rubrospinal tract (rs), and isthmic reticular formation (*is*Rt). (**E**) Mean of the squared Euclidean distance for k-mean's cluster results using cluster number ranging from one to fifteen (x-axis). (**F, top**) Plot spreads showing the anterior-posterior distribution of cue-responsive neurons for each cluster: k1 (n = 33, currant), k2 (n = 59, sky blue), k3 (n = 18, red), k4 (n = 63, blue), k5 (n = 58, orange), k6 (n = 61, dark blue), k7 (n = 64, yellow), and k8 (n = 67, purple). (**F, bottom**) Mean (bar) and individual (data points) baseline firing rate (Hz) for each cluster (colors maintained from F, top). *Independent samples t-test, $p < 0.05$. See also Figure S1 and Figure S3.

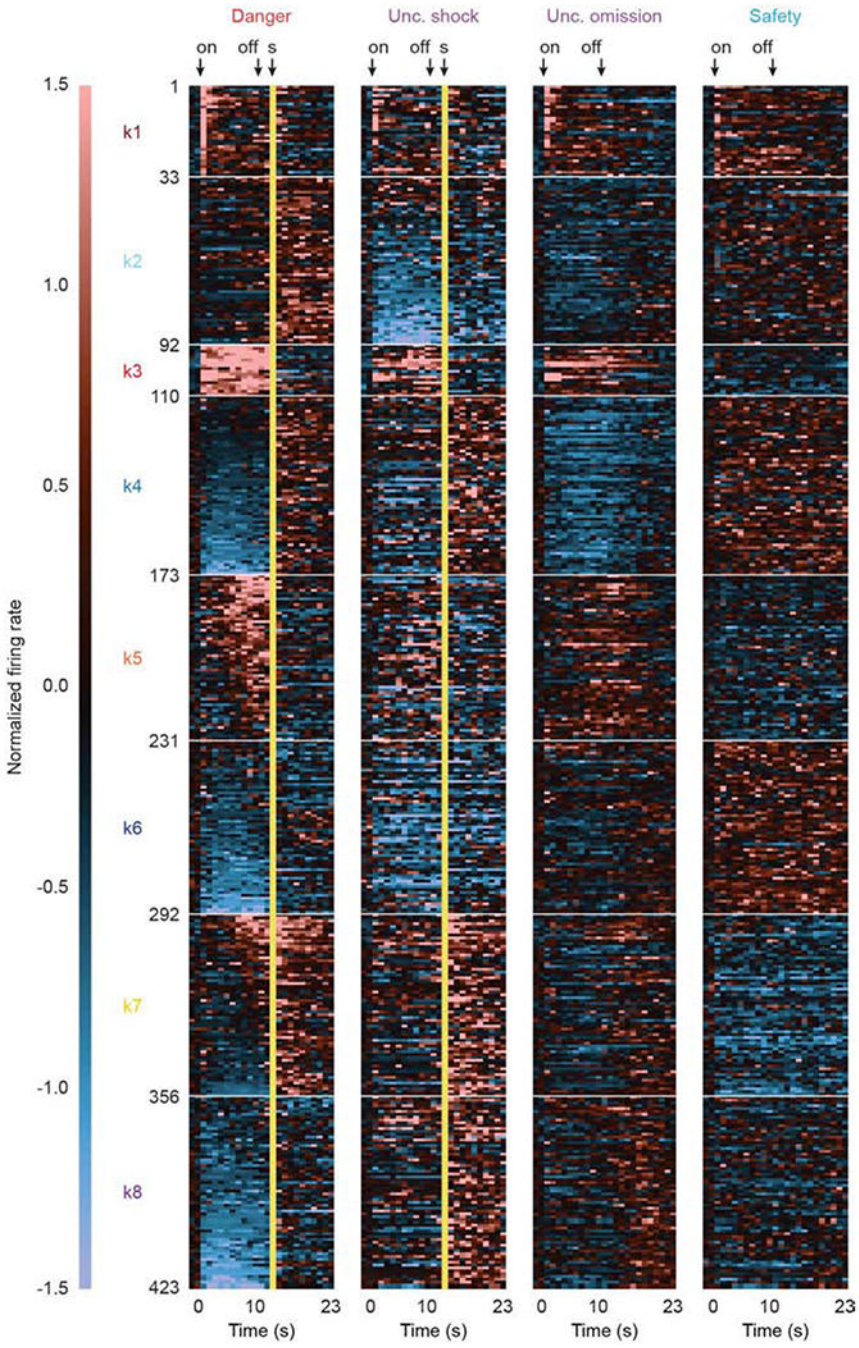

Figure 2. Heat plot and clustering of cue-responsive neurons

Heat plot showing mean normalized firing rate for each cue-responsive neuron (n = 423), from pre-cue through post shock, in 1-s bins for each of the four trial types: danger (red), uncertainty shock (purple), uncertainty omission (purple), and safety (blue). Cue-responsive neurons are divided into eight clusters (k1-8). A normalized firing rate of zero is indicated by the color black, with greatest increases light red and greatest decreases light blue. Cue onset (on) and offset (off) are indicated by black arrows. Foot shock delivery indicated by yellow bars. See also Figure S2.

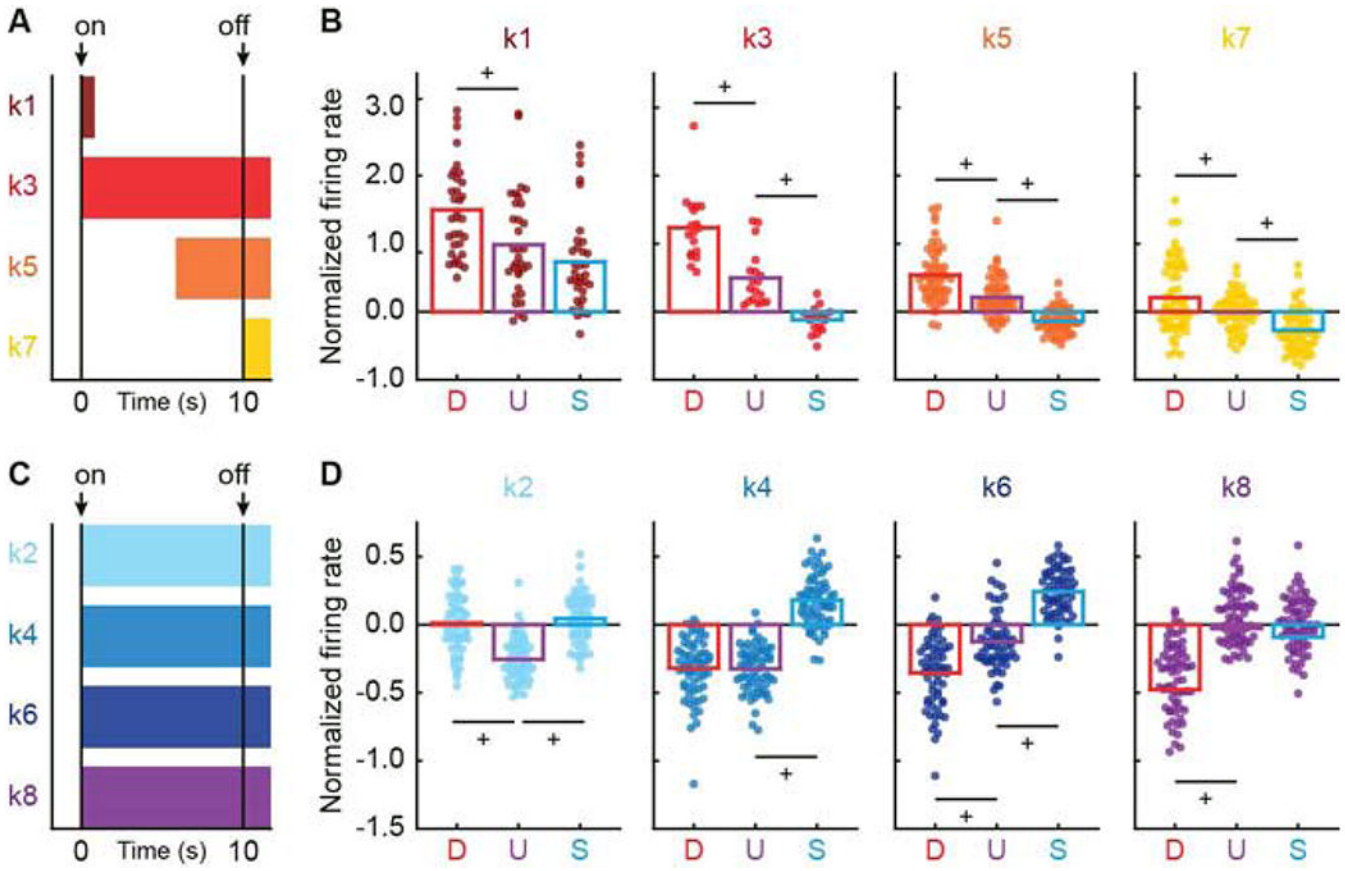

Figure 3. Differential cue firing by cluster

(**A**) Horizontal bars indicate intervals analyzed in B, for clusters: k1 (currant, first 1 s of cue), k3 (red, 10-s cue plus 2 s following cue offset (delay)), k5 (orange, last 5 s of cue plus 2 s following cue offset), and k7 (yellow, 2 s following cue offset). Cue onset (on) and offset (off) are indicated by black arrows. (**B**) Mean (bar) and individual (data points) normalized firing rate for clusters: k1 (n = 33), k3 (n = 18), k5 (n = 58), and k7 (n = 64) are shown for each cue (D, danger, red; U, uncertainty, purple; S, safety, blue). Colors maintained form A. (**C**) Horizontal bars indicate intervals analyzed in D, for clusters: k2 (sky blue), k4 (blue), k6 (dark blue), and k8 (purple). (**D**) Mean (bar) and individual (data points) normalized firing rate for clusters: k2 (n = 59), k4 (n = 63), k6 (n = 61), and k8 (n = 67) for 10-s cue plus 2 s following cue offset, as in B. $^{+}$95% bootstrap confidence interval for differential cue firing does not contain zero. See also Figure S4 and Table S1.

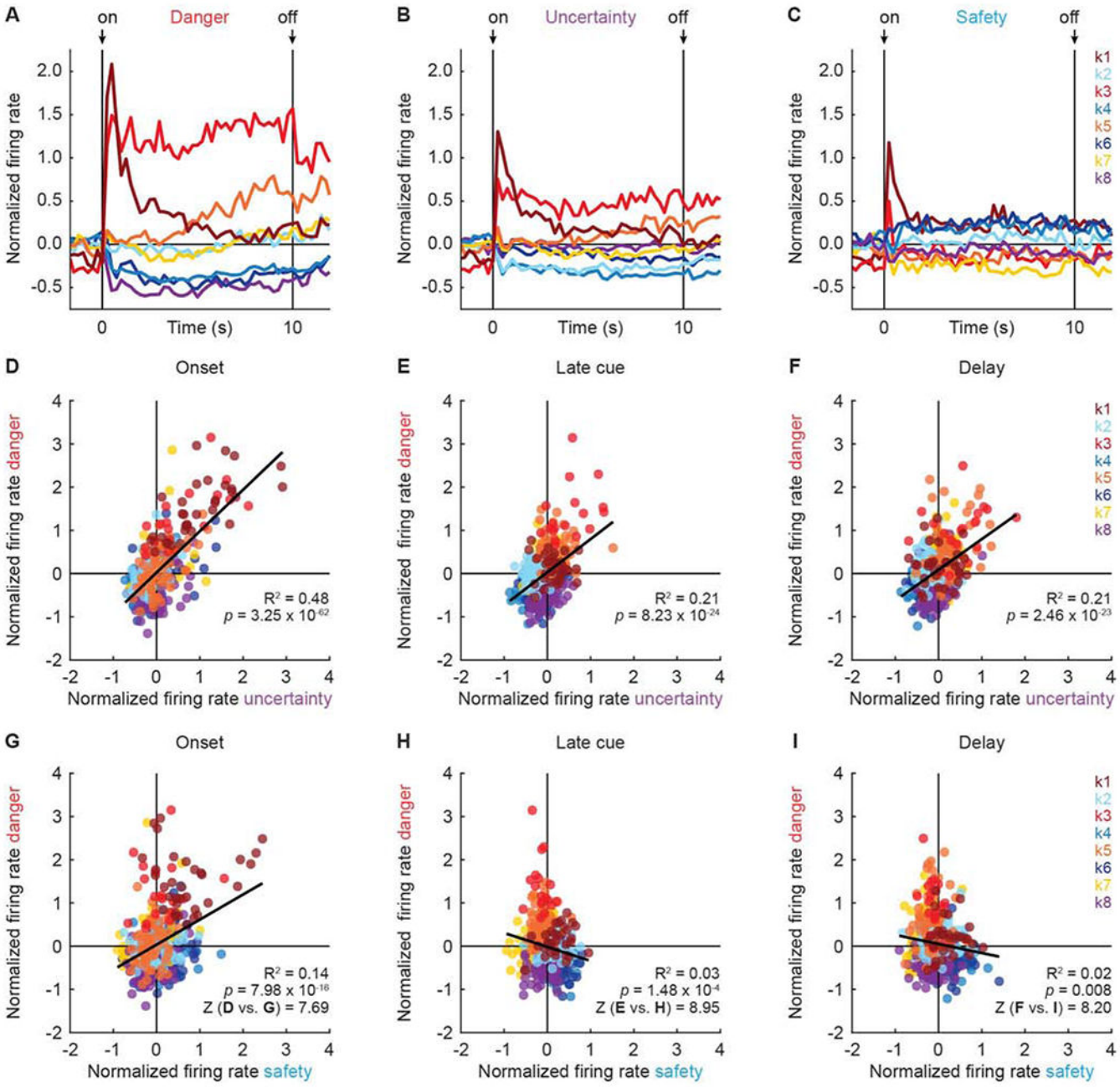

Figure 4. Cue firing across clusters

Mean normalized firing rate from 2 s prior to cue onset, to 2 s following cue offset, is shown for each cluster: k1 (n = 33, currant), k2 (n = 59, sky blue), k3 (n = 18, red), k4 (n = 63, blue), k5 (n = 58, orange), k6 (n = 61, dark blue), k7 (n = 64, yellow), and k8 (n = 67, purple) for (**A**) danger, (**B**) uncertainty, and (**C**) safety. Cue onset (on) and offset (off) are indicated by black arrows. Scatterplots for mean normalized firing rate to danger vs. uncertainty are shown for: (**D**) first 1 s of cue (onset), (**E**) last 5 s of cue (late cue), and (**F**) 2 s following cue offset (delay). R^2 and associated *p*-value (*p*) shown for each correlation. Colors maintained form A. (**G-I**) Scatterplots for mean normalized firing rate to danger vs.

safety shown as in D-F. Danger-uncertainty and danger-safety correlations significantly differed during onset (D vs. G), late cue (E vs. H), and delay (F vs. I). Fisher r-to-z transformation (Z) shown. See also Figure S5.

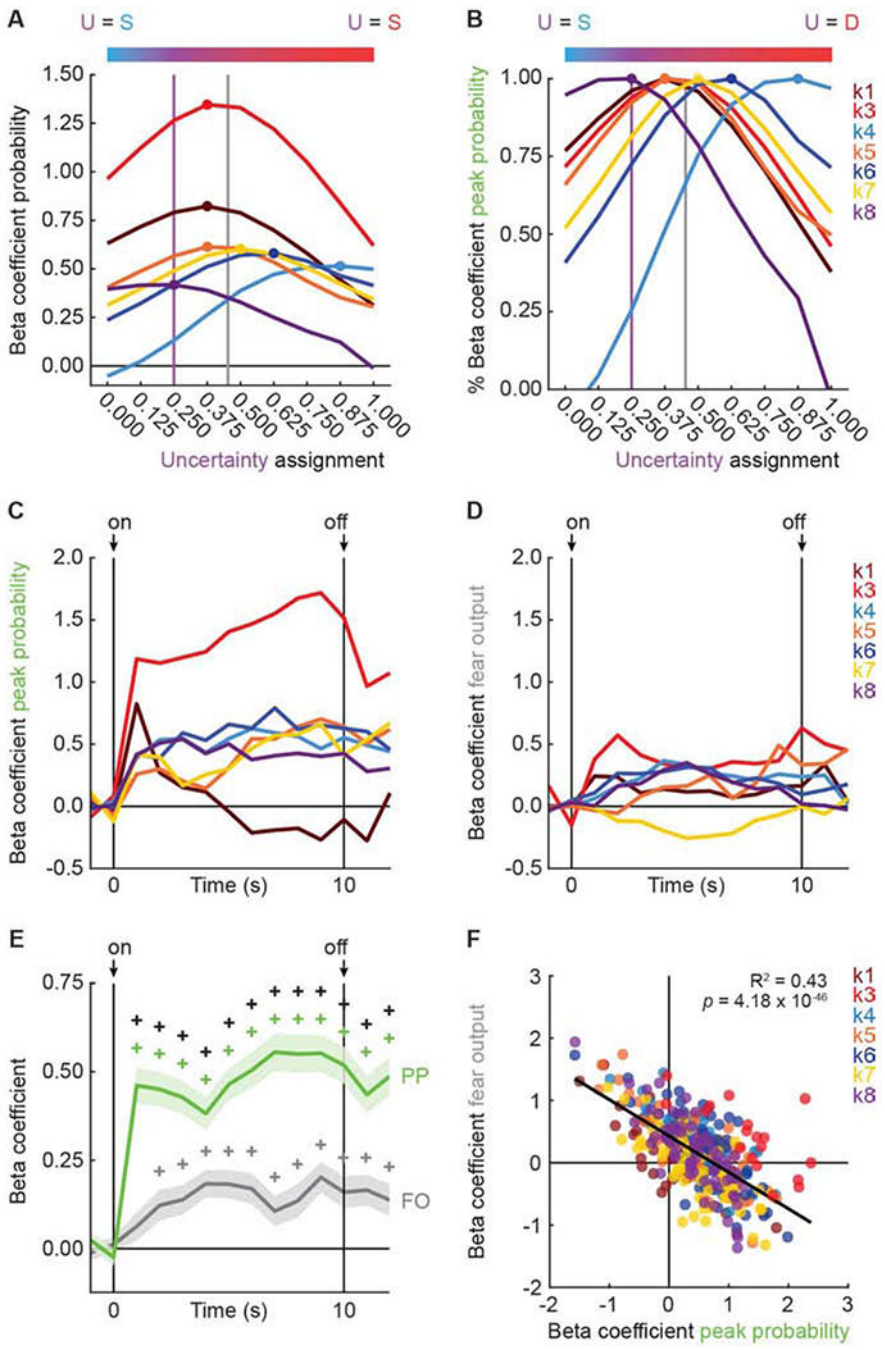

Figure 5. Threat signaling by cue-responsive neurons

(**A**) Tuning curves were constructed for seven of eight clusters: k1 (n = 33, currant), k3 (n = 18, red), k4 (n = 63, blue), k5 (n = 58, orange), k6 (n = 61, dark blue), k7 (n = 64, yellow), and k8 (n = 67, purple). The uncertainty assignment associated with the beta coefficient peak threat probability is indicated with a filled circle. Bar above plots shows a color gradient from safety (blue) to uncertainty (purple) to danger (red). Vertical purple line indicates the actual foot shock probability associated with uncertainty (0.250) and vertical gray line indicates mean fear output to uncertainty. (**B**) Peak threat probability from A expressed as %

of beta coefficient for each cluster (colors maintained form A). (**C**) Mean beta coefficient of peak threat probability is plotted for each cluster over cue presentation. (**D**) Mean beta coefficient of fear output is plotted for each cluster over cue presentation. (**E**) Mean beta coefficients for peak threat probability (PP, green) and fear output (FO, gray) from all seven of eight clusters are plotted. Cue onset (on) and offset (off) are indicated by black arrows. SEM is indicated by shading. (**F**) Mean beta coefficient (fear output) vs. mean beta coefficient (peak threat probability) is plotted for all seven of eight clusters. Trendline, the square of the Pearson correlation coefficient (R^2) and associated *p*-value (*p*) are shown. $^{+}$95% bootstrap confidence interval for differential beta coefficient does not contain zero. $^{+}$95% bootstrap confidence interval for beta coefficient does not contain zero (colored plus signs). See also Figure S6, Table S2 and Table S3.

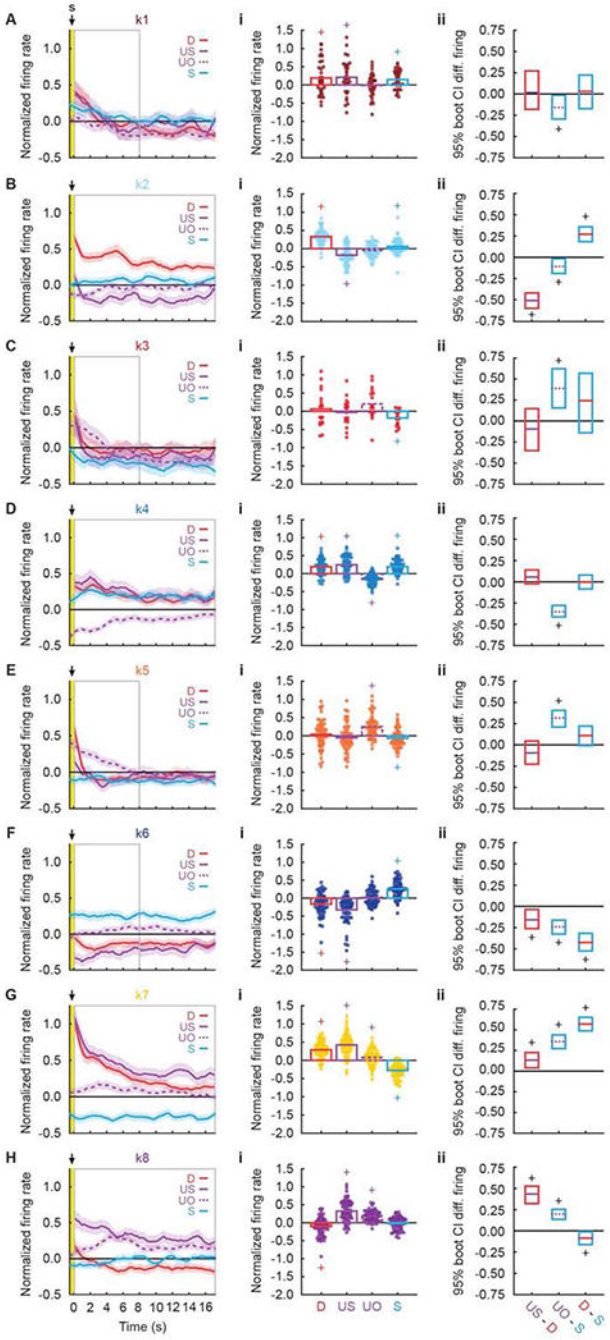

Figure 6. Aversive outcome firing by cluster

(**A, left**) Mean normalized firing rate to danger (D, red), uncertainty shock (US, solid purple), uncertainty omission (UO, dashed purple), and safety (S, blue) is plotted for the 17.5 s following shock offset for k1 neurons (n = 33, currant). Yellow bar indicates shock period and gray box indicates interval analyzed in A, i, ii. Foot Shock delivery is indicated by black arrow. (**A, i**) Mean normalized firing rate for each k1 neurons (data points), as well as the mean for all k1 neurons (bars) is shown for each trial type (colors maintained from above). (**A, ii**) The mean, upper bound and lower bound of the 95% confidence interval (CI)

for differential firing to uncertainty shock vs. danger (left), uncertainty omission vs. safety (middle) and danger vs. safety (right) are shown. Identical plots are constructed for (**B**) k2 (n = 59, sky blue), (**C**) k3 (n = 18, red), (**D**) k4 (n = 63, blue), (**E**) k5 (n = 58, orange), (**F**) k6 (n = 61, dark blue), (**G**) k7 (n = 64, yellow), and (**H**) k8 (n = 67, purple) neurons. $^{+}$95% bootstrap confidence interval for normalized firing rate does not contain zero (colored plus signs). $^{+}$95% bootstrap confidence interval for differential firing does not contain zero (black plus signs). See also Table S4.

Table 1.
ANOVA results for cue and aversive outcome firing by cluster

F statistic, *p*-value (*p*), partial eta squared (ηp^2) and observed power (op) for the trial type x interval interaction for cue firing, as well as for the trial type x interval interaction and main effect of trial type for aversive outcome are provided for each cluster. See also Figure S4, Table S1 and Table S4.

			k1	k2	k3	k4	k5	k6	k7	k8
Cue	Trial Type x Interval Interaction	F	4.00	3.54	4.91	7.93	6.66	7.34	4.64	6.56
		P	**5.93E-38**	**1.38E-31**	**5.57E-49**	**2.82E-110**	**1.82E-86**	**3.75E-99**	**2.42E-50**	**2.33E-85**
		np^2	0.11	0.06	0.22	0.12	0.11	0.11	0.07	0.09
		op	1.00	1.00	1.00	1.00	1.00	1.00	1.00	1.00
Aversive Outcome	Trial Type x Interval Interaction	F	1.23	2.13	1.20	1.83	2.62	1.11	3.83	2.18
		P	**0.02**	**2.21E-18**	**0.03**	**5.86E-12**	**6.98E-31**	0.14	**1.32E-66**	**1.09E-19**
		np^2	0.04	0.04	0.07	0.03	0.04	0.02	0.06	0.03
		op	1.00	1.00	1.00	1.00	1.00	1.00	1.00	1.00
Aversive Outcome	Trial Type Main Effect	F	2.92	56.62	2.12	46.62	3.90	48.82	95.16	47.25
		P	**0.04**	**1.37E-25**	0.11	**1.97E-22**	**0.01**	**3.88E-23**	**2.31E-37**	**4.47E-23**
		np^2	0.09	0.50	0.11	0.43	0.06	0.45	0.61	0.42
		op	0.68	1.00	0.51	1.00	0.82	1.00	1.00	1.00

KEY RESOURCES TABLE

REAGENT or RESOURCE	SOURCE	IDENTIFIER
Antibodies		
Rabbit polyclonal anti-tyrosine hydroxylase	Millipore-Sigma	Cat No. AB152
Biotinylated goat anti-rabbit IgG	Vector Laboratories	Cat No. PK-4001
Bacterial and Virus Strains		
Biological Samples		
Chemicals, Peptides, and Recombinant Proteins		
Avidin	Vector Laboratories	Cat No. PK-4001
Biotin	Vector Laboratories	Cat No. PK-4001
Normal goat serum	Vector Laboratories	Cat No. PK-4001
Hydrogen peroxide	Millipore-Sigma	Cat No. 216763
Vector NovaRED	Vector Laboratories	Cat No. SK-4800
Triton X-100	Millipore-Sigma	Cat No. T8787
Ethylene glycol	Millipore-Sigma	Cat No. 324558-1L
Histo Prep 100% ethyl alcohol	Fisher Scientific	Cat No. HC-800
Paraformaldehyde	Millipore-Sigma	Cat No. P6148
10% Neutral buffered formalin	Fisher Scientific	Cat No. 22899402
Sucrose	Fisher Scientific	Cat No. S5
Sodium chloride	Fisher Scientific	Cat No. S640
Histo-clear II	Fisher Scientific	Cat No. 5089990150
Omnimount	Fisher Scientific	Cat No. 5089990146
Potassium phosphate monobasic	Fisher Scientific	Cat No. P285-500
Potassium phosphate dibasic	Fisher Scientific	Cat No. P288-100
Isoflurane	Covetrus	Cat No. 029405
Carprofen	Covetrus	Cat No. 024751
Ringer’s solution	Covetrus	Cat No. 069176
Lidocaine	Covetrus	Cat No. 002468
Cephalexin	Covetrus	Cat No. 070374
Orthodontic resin regular	Pearson Dental	Cat No. C 22-05-98
Critical Commercial Assays		

REAGENT or RESOURCE	SOURCE	IDENTIFIER
Deposited Data		
Raw and analyzed data	This paper	http://crcns.org/
Experimental Models: Cell Lines		
Experimental Models: Organisms/Strains		
Long Evans rat	Charles River	RRID: RGD_2308852
Oligonucleotides		
Recombinant DNA		
Software and Algorithms		
MATLAB	MathWorks	RRID: SCR_001622
SPSS	IBM	RRID: SCR_002865
Adobe Illustrator	Adobe	RRID: SCR_010279
Adobe Photoshop	Adobe	RRID: SCR_014199
MED PC-IV	Med Associates	RRID: SCR_012156
OmniPlex	Plexon	
Offline Sorter V3	Plexon	RRID: SCR_000012
NeuroExplorer	Plexon	RRID: SCR_001818
Other		
Plexon standard commutator	Plexon	Cat No. 50122
Plexon head stage cable – metal mesh	Plexon	Cat No. 91809–017
Plexon head stage	Plexon	Cat No. 40684–020
Omnetics connector	Omnetics Corporation	Cat No. A79042-001
Green board - moveable array	San Francisco Circuits	Cat No. PCB
Stainless steel ground wire	AM Systems	Cat No. 791400
Formvar-Insulated Nichrome wire	AM Systems	Cat No. 761500
12V DC Lantern battery	RAYOVAC	Cat No. 491G53
6V DC Lantern battery	RAYOVAC	Cat No. 3JFU2
Dustless precision pellets	Bio-Serv	Cat No. F0021